Experimental and numerical analysis of a packed-bed thermal energy storage system designed to recover high temperature waste heat: an industrial scale up

Aubin Touzo, Régis Olives, Guilhem Dejean, Doan Pham Minh, Mouna El-Hafi, Jean-Francois Hoffmann, Xavier Py

Experimental and numerical analysis of a packed-bed thermal energy storage system designed to recover high temperature waste heat: an industrial scale up

Aubin Touzo[a,b,*], Régis Olives[a], Guilhem Dejean[b], Doan Pham Minh[c], Mouna El Hafi[c], Jean-François Hoffmann[b], Xavier Py[a]

[a] CNRS-PROMES Laboratoire PROcédés, Matériaux et Energie Solaire, Tecnosud, Rambla de la Thermodynamique, 66100 Perpignan, France
[b] SAS Eco-Tech Ceram, Espace Entreprises Méditerranée, Rue Edouard Belin, 66600 Rivesaltes, France
[c] Université de Toulouse, IMT Mines Albi, UMR CNRS 5302, Centre RAPSODEE, Campus Jarlard, 81013 Albi, cedex 09, France

Keywords:
Thermal energy storage
Waste heat recovery
High temperature
Packed-bed
Regenerator

A B S T R A C T

An industrial-scale air-ceramic horizontal packed-bed thermal energy storage (Eco-Stock®) has been designed and built by Eco-Tech Ceram and tested during an experimental campaign of 500h. The goal is to provide experimental data and analysis of a horizontal and containerized packed bed TES at high temperature, with performance indicators specific to waste heat recovery. A single charge-discharge at 525°C and 3 cycles at 500°C were carried out (300 kW_{Th} for charge, 350 kW_{Th} for discharge). The unit was able to store up to 1.9 MWh_{Th} in a TES system (1.7 × 1.7 × 3.08 m^3) composed by 16-ton of bauxite ceramic media. The packed bed was able to valorize up to 90% of the heat source, which demonstrates the system ability to recover waste heat up to 525°C at industrial scale. No channeling effect and moderate radial thermal gradient were detected, even though the tank had a horizontal geometry. The plug and play TES presents a non-negligible part of its energy stored in the insulant, which can be recovered during discharge. To take into account such phenomenon, a one-dimension 3 temperature model is proposed. The model fitted well with experimental results, with a root mean standard deviation of the model below 20°C for the temperature profiles.

1. Introduction

The French organization ADEME states that 25% to 60% of the energy that is used for industrial heat needs are wasted [1]. The United States Department of Energy estimates that 20 to 50% of the waste heat are lost in the form of process flue gas. For example, up to 29% of the consumed energy are lost as hot gases in the glass, steel, aluminum and cement industries, from 200 to 1700°C [2]. Recovering waste heat becomes mandatory to improve energy efficiency of energy-intensive industrial processes and contributes to the reduction of CO_2 emissions.

To recover waste heat from hot gases, heat exchangers and regenerators have been used for the past 200 years for continuous energy processes. The regenerators, applied in the glass and steel industries, are used to preheat combustion air and achieve a higher efficiency of the natural gas burner.

However, waste heat recovery exploitation is still limited. Miró et al. studied the technical and economic issues of waste heat recovery, and the mismatch between the production of waste heat and consumption [3]. They mentioned that Thermal Energy Storage (TES) is a key to recover intermittent waste heat. Affordable TES solutions are needed to implement massive waste heat recovery.

The mismatch between power production and consumption also affects concentrated solar power plants, which explains that 80% of the planned CSP constructions have a TES [4]. The most widespread TES technology for solar applications consists in the two-tank molten salt storage system. The molten salt is pumped from a cold tank through a heat exchanger to store the heat coming from the solar fields into the hot tank. The process is latter reversed to run a thermal process. In this technology, the Heat Transfer Fluid is used also as storage medium. However, it is possible to reduce the overall cost by using only one tank [5]. In this unique tank, hot and cold fluid are stored in the same tank, split by a thermal gradient called the thermocline. One more step to reduce the cost is to replace a part of the costly HTF by a low-cost filler material, such as natural rocks [6] or by a recycled material to lower the environmental impact [7,8].

In the literature, several prototypes have been studied, but few were

* Corresponding author.
E-mail address: aubin.touzo@promes.cnrs.fr (A. Touzo).

Notation

Latin letters

C_p	Specific heat [J kg^{-1} K^{-1}]
$\dot{m}$	Mass flow rate [kg h^{-1}]
M	Mass of bauxite [kg]
Q	Enthalpy variation [J]
T	Temperature [°C]
t	Time [h]
x	Axial coordinate of bed [m]

Greek letters

θ	Dimensionless temperature [-]
τ	Load ratio [-]
γ	Cycle efficiency [-]
γ'	Storage yield [-]

Subscripts

amb	ambient
bau	relative to the bauxite pieces inside the packed bed
c	relative to the low-temperature end of the storage
ch	relative to charging phase
d	relative to discharging phase
end	relative to the end of a charge or discharge
exc	exchanged between the inlet air and the system
global	relative to the storage, ducts and diffuser
h	relative to the high-temperature end of the storage
insu	stored inside the wall, or lost to the ambient through it
l	relative to the low-temperature of the storage
local	relative to the storage tank between section A and C
max	maximum
min	minimum
trans	transient: heat flow exiting the system at the outlet
wall_loss	thermal losses associated to the wall

Acronyms

ACAES	Adiabatic Compressed Air Electric Storage
CSP	Concentrated Solar Plant
HTF	Heat Transfer Fluid
PCM	Phase Change Material
RMSD	Root Mean Square Deviation
TES	Thermal Energy Storage

above 1 MWh_{Th} TES capacity. Zunft *et al.* published experimental results of a 9 MWh air/ceramic packed bed thermal storage system, using a honeycomb geometry instead of a packed bed [9]. During 3 cycles, the system was found to be able to deliver air at relatively constant temperature to supply a Rankine cycle at 640-680°C. To the best of our knowledge, the temperature distribution along the bed was not explicitly provided. Zanganeh *et al.* tested a 6.5 MWh_{Th} packed bed TES system, using air as HTF up to 650°C [10]. A one-dimension numerical model with 2 phases (fluid and solid) was validated on a conical TES with a 110 h charging time to evaluate the contribution of radiation and heat losses on the storage. The storage unit was conical and immersed in the ground to withstand the mechanical stress due to the thermal expansion of the particles. The goal was to reveal the potential of packed bed storage for concentrated solar plant (CSP) applications, where a scale-up design of 7.2 GWh unit has been simulated. Geissbühler *et al.* developed a 12 MWh_{Th} packed bed TES system for adiabatic compressed air electric storage (ACAES) application [11]. The shape was slightly conical, to reduce mechanical stress once again. The tests were carried out at 550°C, up to 7 bar. A particular attention is given to the insulant by using one more phase (3 phases in total) to the one-dimension model, which has been validated. Air leakage has been estimated to be close to 15%, due to the void near the walls and due to steel deformation. This latter is a consequence of the high temperature cycling. Recently, Esence et al. investigated two rectangular thermal storage units, a granular packed bed of 1.4 MWh_{Th} and a structured bed of 1.1 MWh_{Th} [12]. The units were charged at 800°C and were subjected to a hundred of thermal cycles. The numerical simulations revealed that the behavior of both units can be accurately predicted during the cycles. Air leakage has been detected due to flow channeling in the corner, causing large heterogeneities in the transverse sections. The rectangular geometry was strongly affected by the mechanical stress, with the fracture of 97% of the structured material and a rupture of the edge of the internal walls for the packed bed storage [13].

Studies on prototypes smaller than 1 MWh_{Th} were used for 3 purposes. The first is to validate the correlation used in the numerical codes (convection, conduction, radiation). All the work regarding numerical computation has been reviewed, presenting different correlations coming from both experimental and theoretical approaches [14]. The second purpose is to experiment different materials or geometries to optimize heat transfer. To go towards cost reduction, cheap natural material such as quartzite has been used [15]. To valorize industrial waste, Ortega-Fernandez *et al.* tested steel slag as filler material with a 400 kWh_{Th} setup, proving its thermal and mechanical stability [16]. The third purpose is to study the influence of operating conditions of thermal storage, such as speed of charge/discharge or operating temperature thresholds. Fasquelle *et al.* showed that the use of a dynamic temperature threshold for an interconnected thermal storage should be preferred to the arbitrary temperature threshold for CSP application [17].

In the past years, horizontal configurations were tested as a way to facilitate the implementation on site. Ferber *et al.* built a first experimental setup of 45 kWh_{Th} with a horizontal geometry. They defined specific indicators for waste heat recovery, as opposed to those used for solar applications. They also looked at the influence of degraded conditions on the charge and discharge of the storage, by varying the temperature and the flowrate [18]. The degraded inlet flow had no effect on the performances of the storage. The geometry of this experimental setup was then scaled up to reach an industrial size for the purpose of this study. Al-Azawii *et al.* noticed a performance increase with the flowrate on a similar geometry prototype, explained by lower heat losses during charging and discharging time [19]. Soprani *et al.* built a lab-scale (450 kWh_{Th}, 27 kW_{Th}) horizontal rock bed system [20]. They presented the horizontal configuration as promising for upscaling the packed bed TES for two reasons: a cheaper and less complex design and a significant reduction in the excavation cost for integrating the rock bed into the ground. However, buoyancy forces reduced the performances of the storage. They found that raising the flowrate improved the performances, reducing the buoyancy forces with the flow inertia. To further reduce buoyancy, they also tested to split the packed bed horizontally with layers of insulant. They supposed that industrial units could recover 90 to 95% of the heat. At the best of our knowledge, only one large size horizontal TES provides data [21,22]. Instead of using packed bed, they used hollow bricks to lower pressure losses. The dispersion concentric model was used to model the solid with a Biot number superior to 1. They did not find any thermal discrepancies between the top and the bottom. TES performances indicators, such as storage yield, were not defined in the study. Last, the project of Siemens Gamesa in Hamburg can also be mentioned, with a nominal capacity of

120 MWh. However, no data were published.

The French company Eco-Tech Ceram is specialized in the design and construction of innovative TES systems. They have built the Eco-Stock®, a containerized and mobile TES system for waste heat recovery that can store and recover heat up to 600°C, at at least 300 kW_{Th}. As outlined by the literature review, no data regarding horizontal large packed bed TES is available. Thus, the objective of this study is to provide experimental data of a horizontal and containerized packed bed TES at large scale (28 tons, 1.9 MWh_{Th} capacity), at a temperature equivalent to molten salt TES. The performances of this singular TES can be measured thanks to indicators for open loop waste heat recovery systems, such as load ratio or storage yield.

Smaller units present large edge effects, that requires a 3 temperature model (solid, fluid, wall). For industrial scale unit, edge phenomena were supposed to be neglected, the ratio between insulant and storage material being reduced. However, the plug and play TES studied here presents a non-negligible part of its energy stored in the insulant. This energy is not lost, since it can be recovered during the discharge. Thus, a 1 dimension 3 temperature model is proposed to take into account those edge effects.

2. Experimental Setup

2.1. Test bench description

The main structure of the test bench is made up of 3 elements: an electrical cabinet, an air heater skid and a TES system. The skid comprises an air inlet, a fan, an electric air heater, a chimney and valves allowing or not the air to flow to the TES system. Heat is generated using electric heaters with a 480 kW_e capacity. The inlet TES tank dimension is 3.08 m × 1.7 m × 1.7 m (8.9 m^3) which can fit into a 20-feet container. The total mass is 28 tons, enabling transport by truck. The Eco-Stock® used in this work can store heat up to 600°C, using 16 tons of a commercial refractory ceramic, which is bauxite rubbles (characteristic diameter 30 mm, bed porosity 40%). The tank is insulated using 200 mm of refractory bricks. Figure 1 shows a picture of the test bench composed by the TES system, the electric cabinet, and the air heater skid.

Eco-Tech Ceram designed a horizontal packed bed inside a container. This horizontal geometry facilitates the implementation of the TES on site for waste heat recovery. Lopez Ferber *et al.* built a horizontal experimental setup, which was the first step leading to a containerized Eco-Stock® [18]. The radial temperature revealed to be homogeneous, which means that the thermocline was not altered by the horizontal configuration on the tested range of flowrate (39, 72 and 123 $kg.s^{-1}$). However, thermal alterations would be likely to appear on an industrial storage unit because of longer charging periods. Moreover, Esence *et al.* showed the issues related to thermal ratcheting [13]. These can be solved by using a horizontal geometry which would decrease the pressure on the walls, by increasing the ground area. However, all geometries in the literature are vertical to preserve the thermocline with the natural convection process.

Figure 2 shows the principle of the charging and discharging steps of the Eco-stock®. The charging step was already detailed elsewhere [18].

Briefly, the air at room temperature enters the setup by the air inlet, via a 30 kW_e fan. This air is sent to a 480 kW_e electric air heater before going through the thermal storage medium. The HTF comes back to the skid thanks to a return air duct, leading the cold air to the chimney. The return air duct is located inside the container. For the discharging step, the HTF flux can be reversed thanks to the valves (V1, V2, V3, V4, and V5). The air at room temperature directly enters the TES system, discharging the latter while generating hot air.

2.2. Instrumentation

The TES instrumentation is made of 33 K-type thermocouples (precision +/- 2.2°C). The thermocouples are inserted into a perforated ducting system implemented on one side of the storage. 9 thermocouples are positioned along the TES, to obtain the temperature profile. As it can be seen on Figure 3, the first is located 100 mm from the hot zone entrance in the filler material, and the last located 100 mm from the cold zone. The others are spaced of 360 mm from each other. Inlet air temperature is also followed thanks to 1 thermocouple at each end of the set-up.

The transversal temperature is measured in 3 sections A, B and C, located respectively at 100 mm, 1540 mm and 2980 mm from the entrance. 9 thermocouples were used for each section. The top and bottom thermocouples were situated at a 150 mm depth into the storage bed. The right and left were situated at a 150 mm depth into the storage bed.

The position of the thermocouples was chosen to carry out thermal balance on the unit, from a process engineering point of view. Therefore, no particular focus was put on temperature heterogeneity, but rather to get a temperature representative of the cross-section. Nevertheless, the top and bottom thermocouples still enable detecting flow heterogeneities that would be caused by channeling or natural convection (buoyancy forces are not limited in a horizontal configuration).

The entrance temperature of the air was measured at 500 mm after the air heater collector represented by T1 on Figure 2. Another measurement of the temperature was also done at the end of the return air duct represented by T2, about 4 m after leaving the TES system. The

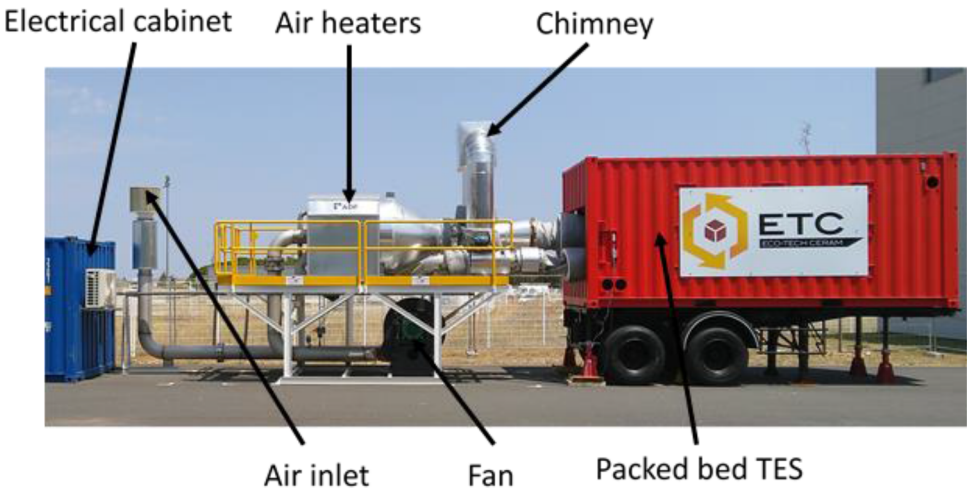

Figure 1. Commented picture of the setup.

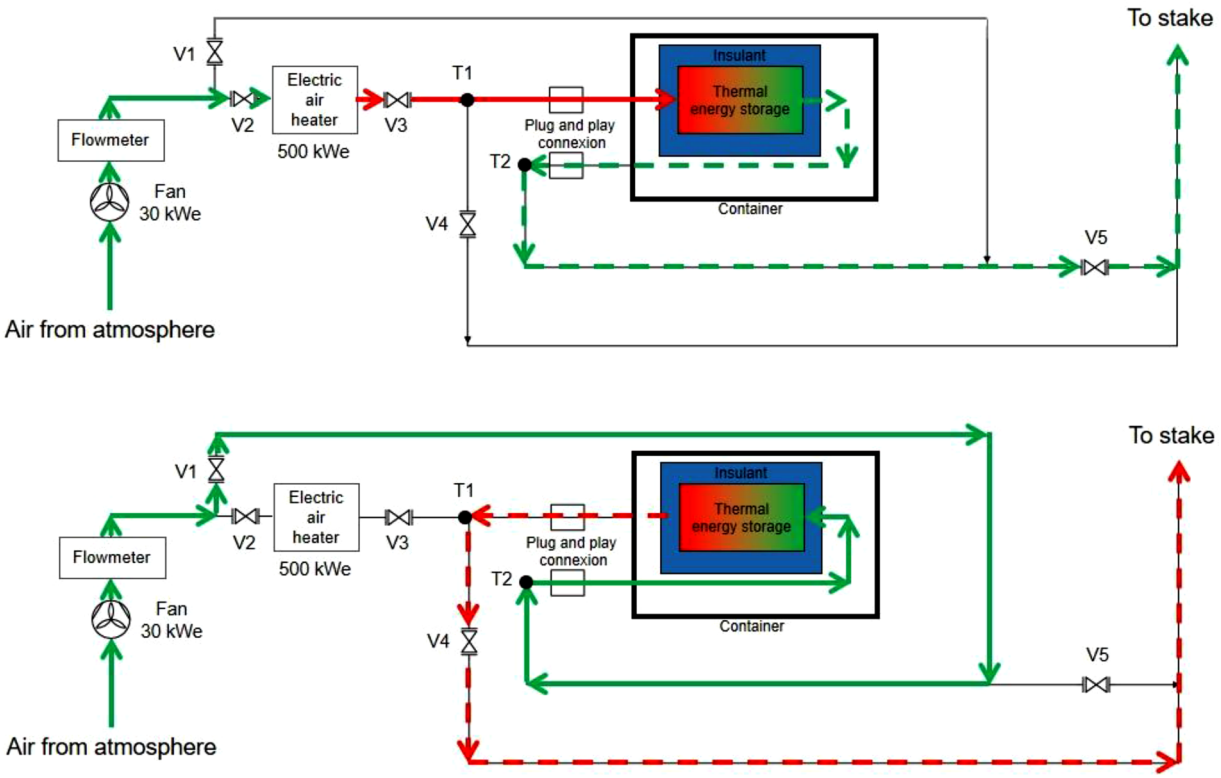

Figure 2. Charging (top) and discharging (bottom) process.

ambient temperature was also measured. No measurement of the temperature was done inside the insulant.

3. Indicators

Definitions of energy indicators for open system TES were proposed by Lopez Ferber [18]. The same definitions are used here to be able to compare both systems. The definition of the yield is particularly important since an open system can lose energy to stake as waste heat.

To compare different systems behavior at different operating temperatures, the dimensionless temperature can be a practical parameter, defined commonly in the literature as follows:

$$\theta = \frac{T(t) - T_l}{T_h - T_l} \tag{1}$$

T_l is the ambient temperature.

The enthalpy supplied to the system is the enthalpy difference between the high temperature heat source and the ambient air, given by equation 2:

$$Q_{air-ch}(t) = \int_0^t \dot{m}(t)\left(\int_{T_l}^{T_h(t)} Cp_{air}(T)dT\right)dt \tag{2}$$

The heat $Q_{air\text{-}ch}$ could be stored by the TES material Q_{bau}, by the insulant $Q_{lateral}$, and lost through the chimney Q_{trans}.

The enthalpy stored by the TES material corresponds to the rise in temperature compared to the initial state. The 9 thermocouples define 9 sub-volumes of the storage medium. The temperature is assumed homogeneous in each sub-volume.

$$Q_{bau}(t) = \sum_{i=1}^{n} \int_{T_i(0)}^{T_i(t)} Cp_{bau}(T)M_i dT \tag{3}$$

With T_i the temperature of the i^{th} sub-volume M_i the mass of the i^{th} sub-volume and n equals 9.

The properties of bauxite and air varies with the temperature. For each property X(T) (c_p, λ, ρ), the following equation is used:

$$X(T) = \sum_{0}^{n} a_i T^i \tag{4}$$

with a_i constants given in Table 1:

The air properties come from correlations given by Agalit *et al.* [23]. The heat capacity, thermal conductivity and density of the bauxite in the temperature range of 25-1000°C were ordered to Netzsch Applications Laboratory (France). The equipment were NETZSCH laser flash apparatus LFA 467 HT HyperFlash® and NETZSCH model DSC 404 F1 Pegasus®. The density was obtained by buoyancy flotation method at room temperature.

Equation 5 defines the load ratio. In this equation, $Q_{bau}(t)$ is the energy received by the system which depends on the temperature of the TES material during the charging step, and $Q_{bau\text{-}max}$ is the charging capacity of the TES when the system reaches its highest temperature (525°C).

$$\tau(t) = \frac{Q_{bau}(t)}{Q_{bau-max}} \tag{5}$$

Since the setup is an open system, heat can be dissipated downstream the TES to the chimney. The enthalpy that transited through the storage without being stored is calculated between the temperature from the cold side of the storage and the ambient temperature. The transited energy was calculated with equation 6:

$$Q_{trans}(t) = \int_0^t \dot{m}(t)\left(\int_{T_l(t)}^{T_c(t)} Cp_{air}(T)dT\right)dt \tag{6}$$

A part of the inlet energy can also be stored in the insulant $Q_{lateral}$. The refractory insulant material has a density of 480 $kg.m^{-3}$ and a specific heat of 1.05 $kJ.kg^{-1}.K^{-1}$ (at 1000°C), and therefore cannot be neglected (estimated to 6% of TES capacity). Because neither the temperature of the external wall nor the temperature inside the insulant

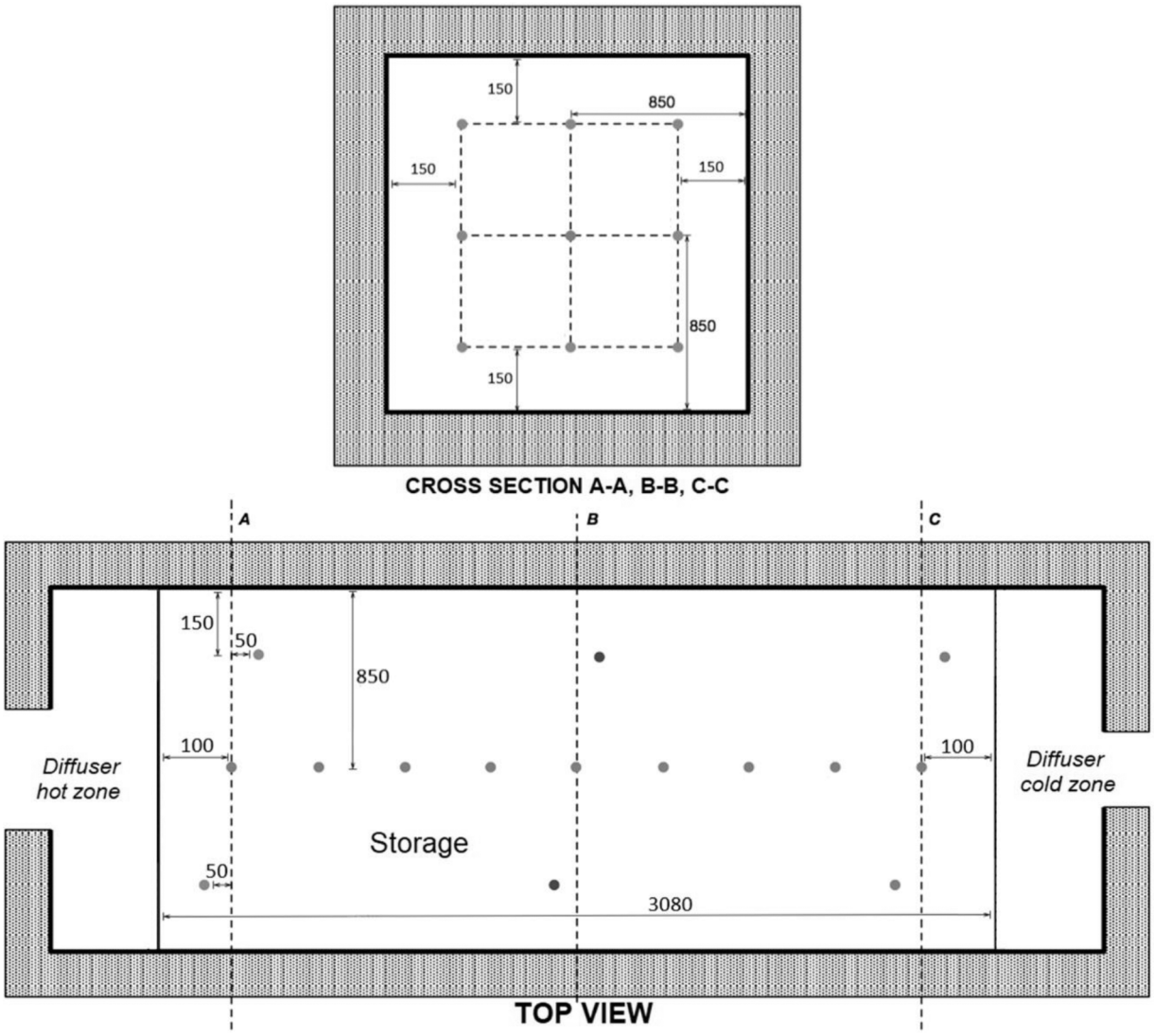

Figure 3. Instrumentation of the TES.

were measured, it is not possible to assess the distribution between the latter and the convection losses. In addition, Q_{bau} takes only into account the temperatures measured by thermocouples located in the middle of the tank. A migration of the heat by natural convection would decrease the energy in Q_{bau}, but the energy stored in the tank would be the same. So, in this work, $Q_{lateral}$ cannot be measured, but it is only calculated by the following equation:

$$Q_{lateral}(t) = Q_{air-ch}(t) - Q_{trans}(t) - (Q_{bau}(t) - Q_{bau}(t=0)) \quad (7)$$

The enthalpy discharged is calculated between the temperature from the hot side of the storage and the ambient temperature. The discharged energy is calculated by the equation 8 below:

$$Q_{exc-d}(t) = \int_0^t \dot{m}(t)\left(\int_{T_l(t)}^{T_h(t)} Cp_{air}(T)dT\right)dt \quad (8)$$

The piping depends on the distance of the waste heat source, which depends on the industrial site and could impact energy balance calculation. Therefore, in order to evaluate the storage performance of the system, two different indicators are defined. The first one, named global storage yield, considers all the elements of the TES system.

Table 1
Air and bauxite properties.

Coefficient	Air [21] C_p ($kJ.kg^{-1}.°C^{-1}$)	λ ($W.m^{-1}.K^{-1}$)	ρ ($kg.m^{-3}$)	Bauxite C_p ($kJ.kg^{-1}.°C^{-1}$)	λ ($W.m^{-1}.K^{-1}$)	ρ ($kg.m^{-3}$)
a_0	1.006E+03	2.477E-02	1.274	7.527E-01	5.070	3.005E+03
a_1	-8.615E-03	7.30E-05	-4.509E-03	1.531E-03	-4.950E-03	-
a_2	6.581E-04	-2.59E-08	1.34E-05	-1.850E-06	5.423E-06	-
a_3	-7.13E-07	9.38E-12	-2.80E-08	8.890E-10	-2.518E-09	-
a_4	2.42E-10	-	3.56E-11	-	-	-
a_5	-	-	-2.43E-14	-	-	-
a_6	-	-	6.75E-18	-	-	-

$$\gamma_{global}(t) = \frac{Q_{exc-d-global}(t)}{Q_{air-c-global}(t_{end-ch})} \quad (9)$$

The second one, named local storage yield which is based on a TES system approach. Thus, it can be applied to any other system. In this case, the system is only considered between the sections A and C (Figure 3) where the temperature was experimentally measured.

$$\gamma_{local}(t) = \frac{Q_{exc-d-local}(t)}{Q_{air-c-local}(t_{end-ch})} \quad (10)$$

4. Description of the numerical model

The numerical models the storage as porous media. The one dimensional numerical model consists in 3 coupled energy equations, for the fluid, solid, and wall, as developed by Ismail and Stuginsky [24] and Hoffmann *et al.* [25]. It is assumed that the air is properly and homogeneously distributed via the diffuser without radial effect. Those hypotheses will be checked afterwards. The bauxite rubble temperature is assumed to be homogeneous since the Biot number is inferior to 1, calculated at 0.1.

$$\varepsilon(\rho c_p)_{air}\left(\frac{\partial T_{air}}{\partial t} + u\frac{\partial T_{air}}{\partial x}\right) = \frac{\partial}{\partial x}\left(k_{air-eff}\frac{\partial T_{air}}{\partial x}\right) + h_v(T_{bau} - T_{air}) + h_w\frac{A_{air\leftrightarrow w}}{(V_{air}+V_{bau})}(T_w - T_{air}) \quad (11)$$

$$(1-\varepsilon)(\rho c_p)_{bau}\frac{\partial T_{bau}}{\partial t} = \frac{\partial}{\partial x}\left(k_{bau-eff}\frac{\partial T_{bau}}{\partial x}\right) + h_v(T_{air} - T_{bau}) \quad (12)$$

$$(\rho c_p)_w\frac{\partial T_w}{\partial t} = \frac{\partial}{\partial x}\left(k_w\frac{\partial T_w}{\partial x}\right) + h_w\frac{A_{air\leftrightarrow w}}{V_w}(T_{air} - T_w) + h_{ext}\frac{A_{w\leftrightarrow ext}}{V_w}(T_{ext} - T_w) \quad (13)$$

Fluid (air) and solid properties injected to the model are recovered from the Section 3.

Regarding the boundary conditions, the temperature is imposed at the inlet while adiabatic condition is imposed at the outlet. $k_{bau\text{-}eff}$ takes into account the porosity and the radiation between successive solid particles. All correlations that are used to estimate the heat transfer coefficients can be found in the work of *Esence et al.* [14]:

$$h_v = \left(2 + 1.1Re^{0.6}Pr^{\frac{1}{3}}\right)\frac{k_{air}}{d} \quad (14)$$

$$h_w = \left(0.203Re^{\frac{1}{3}}Pr^{\frac{1}{3}} + 0.203Re^{0.8}Pr^{0.4}\right)\frac{k_{air}}{d} \quad (15)$$

$$h_{ext} = (0.664Re_{ext}^{0.5}Pr_{ext}^{1/3})\frac{k_{air}}{D} \quad (16)$$

$$k_{air-eff} = \varepsilon k_{air} + k_{eff}^{R} \quad (17)$$

$$k_{bau-eff} = (1-\varepsilon)k_{bau} \quad (18)$$

The radiative effective conductivity is chosen from Sih and Barlow [26], as reviewed by Diaz-Heras [27].

The equation system is then solved using implicit finite difference. The scheme applied is centered for the second order derivative and backward for first order derivative.

The thermocouples measure experimentally the air temperature inside the storage. Therefore, the numerical temperature given in this work is the fluid temperature. It can also be noted that thermal inertia caused by the air ducts located between the heat generator and the storage unit is not taken into account.

A part of the flow by-passes the storage medium during charge through valve V1, and leaks occurs through V5 leading the air to the chimney during discharge. A correction is applied to the flowrate to take the leaks into account through an energy balance between the energy stored by the packed bed and the energy provided by the air. The same corrections are applied for single and cycled operation of the TES. For a charge which is operated at 0.68 kg.s^{-1} (precision 1.5%), the correction is estimated at -15% (0.58 kg.s^{-1}). Indeed, the air heater creates a high pressure drop (110 mbar, precision 0.1%), which causes a bypass of the flow through the valves. During the discharge, the pressure drop is only up to 10 mbar, which reduces the flow bypass to only 4% (0.65 kg.s^{-1}).

5. Results and discussions

5.1. Single charge and discharge

This section analyses the results of a charge at inlet temperature of 525°C. The storage was designed to reach 600°C, but the air heater outlet temperature was limited to 525°C. The air flow rate was set at 0.58 and 0.65 kg.s^{-1} for charging and discharging steps respectively (300 kW_{Th} and 350 kW_{Th} for charge and discharge). The threshold charging temperature was set at 190°C. The 190°C threshold matches with the temperature limit of the pre-selected fan. Indeed, the fan would be located on the cold side of the setup on an industrial site. When the outlet air reaches the threshold temperature, the charging process is stopped, the valves are switched to the discharging configuration. The discharge continues until the 200°C threshold (set arbitrarily) is reached.

5.1.1. Temperature evolution

One advantage of the vertical TES is related to the natural convection, which helps to preserve a thin thermocline, the hot zone being on top. This advantage could turn into a drawback on a horizontal geometry, since the natural convection contributes to the de-stratification, with supposedly higher temperature for the top thermocouples and lower for the bottom thermocouples. Therefore, the one-dimension hypothesis can be questioned on a horizontal geometry. The natural convection, potentially coupled with the channeling effect, are likely to bring radial discrepancy of the temperature.

Thermocouples of cross-section B are plotted during the charge on Figure 4. Cross-section B is adequate to look for radial temperature discrepancy, since this cross-section is located in the middle of the storage, far from the inlet and outlet of the storage that might bring side effects.

The temperature of the 9 thermocouples presents a maximum standard deviation of 30°C during the whole charge, with a 16°C

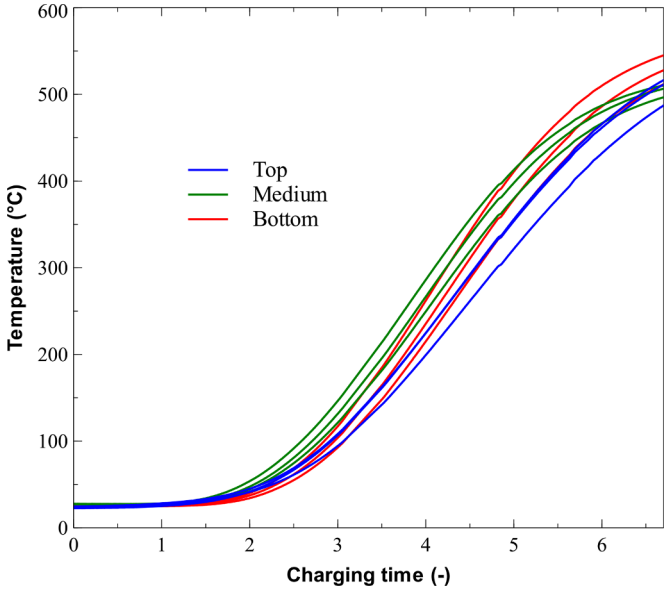

Figure 4. Temperature evolution of thermocouples in cross-section B.

average. The highest temperature is 544°C and the lowest 485°C at the end of the charge. From a process engineering point of view, 60°C seems acceptable to assume a temperature homogeneity in the section and carry out the thermal balance to calculate the performances of the unit.

Esence *et al.* observed a thermal discrepancy of 250°C in the corner of the tank, indicating high velocities due to the channeling effects [13]. This phenomenon is absent in this study, since the thermocouples temperature is relatively homogeneous, meaning an equal distribution of the fluid velocity along the cross section. An explanation could be that the tank has borne vibrations during transportation, which probably improved the distribution of the bauxite rubbles in the corners. Under these particular operating conditions, the horizontal geometry presents similar thermal discrepancy compared to vertical geometry. The same conclusions were made by Lopez-Ferber on a prototype unit [28].

To have an overview about radial discrepancies in the whole storage, the root mean square deviation (RMSD) of the model is calculated for each thermocouple during the charge, and is presented on Figure 5.

For the section A, three thermocouples at the bottom showed the highest RMSD compared to those at the middle and top, which is the opposite of what was expected. This is probably due to a defect in the diffuser, or a heterogeneity in the flow. Indeed, the flow is probably not stabilized since the diffuser is located about 1.5 m downstream the air heater. This phenomenon could be coupled with channeling effects, even though the horizontal geometry provides a good distribution of the sphere at the bottom on the tank. All those effects are not modeled, which explains a high deviation in section A. The RMSD are lower at section B compared to section A, especially for the centered middle thermocouple with a 5.3°C deviation average. This homogenization comes from the packed bed itself and a few diameters of particles length are probably necessary to homogenize the mass flow over the section. However, due to edge effects such as channeling effect, the temperature deviation reaches 28.9°C for the top and 21.1°C for the bottom thermocouples. The channeling effect is still very limited compared to the high charging temperature of 525°C. Section C revealed a low RMSD of 7.2°C for the centered middle thermocouple. The average RMSD for the top thermocouple is 24.2°C, which indicates a moderate thermal radial effect.

Similar RMSD are observed during discharge, with 8.7°C, 16.6°C and 13.1°C respectively for the middle thermocouples of section A, B and C respectively.

The model is able to predict accurately the temperature along the tank, especially in the center of the tank, and presents low radial heterogeneities, apart section A, where the flow is not properly distributed.

Since no higher temperatures can be seen in the charging phase in section A, B or C, the impact of natural convection seems negligible. Heat exchange is driven by forced convection which decreases the impact of the natural convection. In this case, the one-dimension hypothesis can stand, and the experimental results presented here can be used to validate one-dimension numerical model independently of the vertical or horizontal geometry of the tank.

Figure 6 shows both experimental (points) and numerical results (continuous lines) during the first charging and discharging. The temperature measured in the central positions along the bed are plotted every hour during the charging and discharging steps.

The idle phase between charge and discharge lasted 25 min. Globally, numerical results fitted well experimental points which indicates that the TES performances were consistent to the design. During the first hours of charging, the thermocline entirely occupied the tank, similarly to the observation of Esence *et al.* [13]. At the end of the charge, the temperature was constant at 525°C (feeding temperature) in the first meter length of the tank. Reducing from 30 to 10 mm would increase of the storage capacity of 2.5% (42 kWh). Indeed, the thermocline length would be thinner with TES material of smaller size, as it increases heat exchange surface between the fluid and the solid [29]. However, this solution would also increase pressure drops (from 3.3 to 13.4 mbar) and so costs linked to the fan (capital and operational expenditures) of the setup.

Even though the packed bed geometry is horizontal, the one dimensional model fitted well experimental results.

5.1.2. Load ratio

The temperature profiles seem to match between experimental and numerical approach, the performances indicators defined in Part 3 can now be compared. The load ratio is plotted on Fig. 7 to check the thermal storage charging performance, defined by equation 4. The A and C temperatures are the centered middle thermocouple of section A and section C.

On industrial site, the fan would have been located on the other side of the storage, sucking the flow instead of blowing it into the TES. This configuration keeps the temperature low at the fan, which reduced its associated CAPEX. Therefore, the return air duct has been designed at 200°C, in accordance with the fan. The threshold charging temperature was set to $\theta_{threshold\text{-}ch} = 0.34$ (190°C), using a 10°C margin. 190°C presents a good compromise between heat lost downstream the storage and its load ratio, which reached 77% at the end of the charge.

The load ratio linearly rose until the temperature of the section C started to rise. The temperature of the section A needed approximately 2 hours to reach the charging temperature, which corresponds to the thermal inertia of the duct upstream the TES system and the first 0.1 m

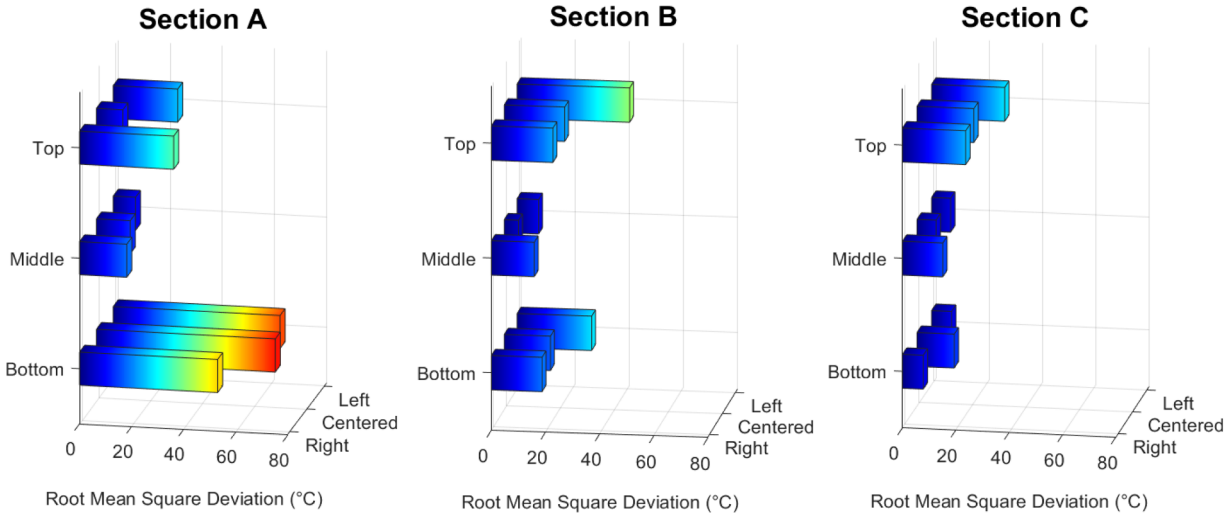

Figure 5. Temperature deviation between numerical and experimental on section A, B and C during charge.

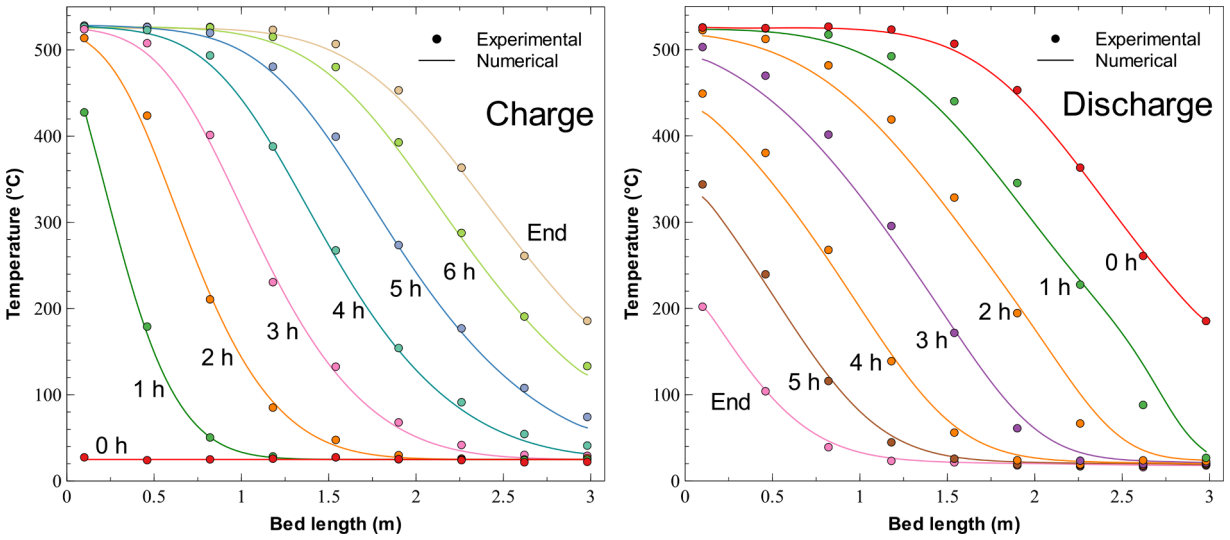

Figure 6. Temperature profile during charge and discharge, when charging step was performed with hot air heated to 525°C.

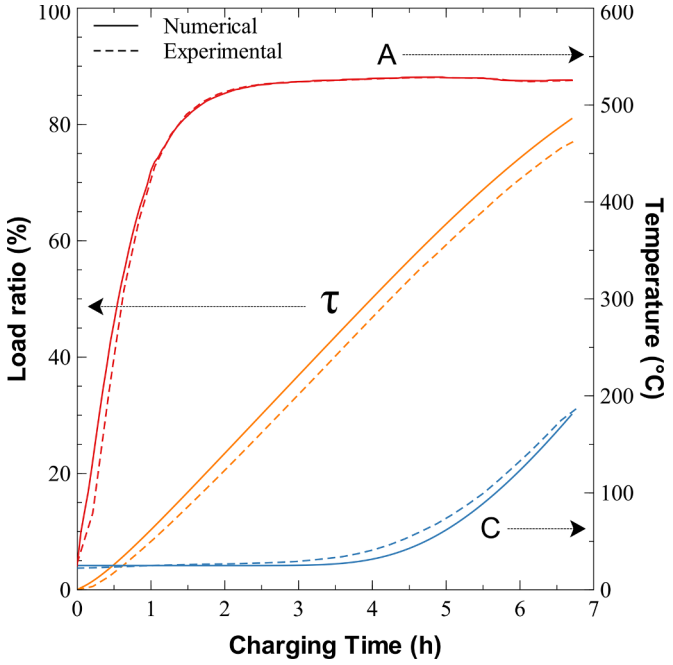

Figure 7. Evolution of the load ratio and the temperature at two sections A and C.

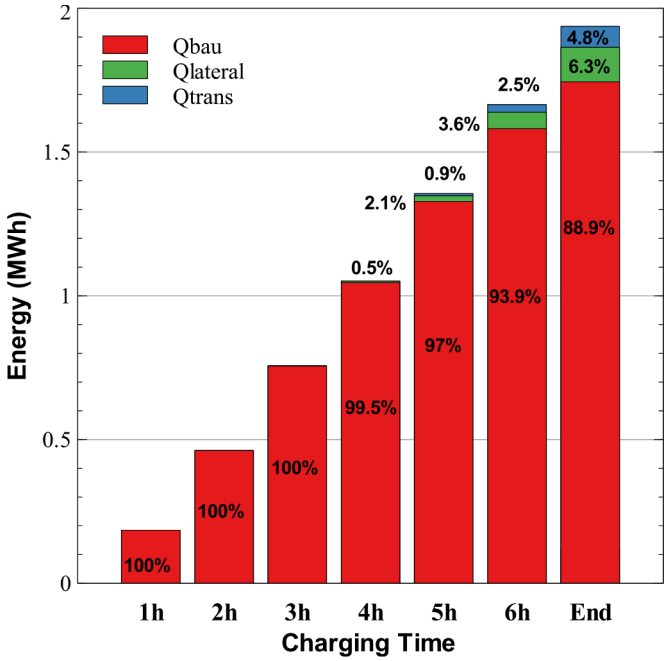

Figure 8. Evolution of the enthalpy supplied to the TES.

of layer before section A. The temperature of the section C remained at ambient temperature during the first four hours, when the thermal gradient (thermocline) started to be extracted from the packed bed.

The load discrepancy between experimental (77%) and numerical (81%) results is likely to come from the calculation of the experimental load ratio. Indeed, the packed bed is divided in 9 sections (one for each thermocouple along the bed), and the bed temperature is assumed constant on these sections (respectively 36 cm between thermocouple). More thermocouple would be needed to get more accurate results.

Increasing the threshold temperature would reduce the final thickness of the thermocline by extracting it from the TES system, which would raise the load ratio, but would also reduce the storage yield. The chosen threshold value enables reducing lost heat to the gas chimney.

5.1.3. Thermal energy repartition

The goal of the Eco-Stock® solution is to recover heat. Therefore, the energy released at the outlet of the storage, Q_{trans}, should be as low as possible. Figure 8 shows the experimental energy balance as a function of the charging time, calculated from the experimental data.

After 1 h of charging, the quantity of energy stored by the TES material Q_{bau} reached 0.18 MWh_{Th}. Between 1 h and 4 h of charging, the rate of energy storage practically reached 0.3 MWh_{Th} per hour. The first hour did not reach 0.3 MWh_{Th} probably due to the absorption by the air duct.

Hot air released to the chimney started around 4 h of charging and reached 4.8% at the end of the charging step. Tests carried out by Lopez-Ferber et al. on a smaller unit revealed 4% loss with $\theta_{threshold\text{-}ch} = 0.2$ and up to 29% loss with $\theta_{threshold\text{-}ch} = 0.8$. $\theta_{threshold\text{-}ch} = 0.34$ presented a compromise between τ and Q_{trans}, with a threshold temperature of 190°C.

The quantity of energy stored in the insulant, $Q_{lateral}$, was significantly observed from 5 h of charging and got a value of 6.3% at the end of the charging step. This energy is not really a loss, since a part of the energy stored in the insulant is recovered during the discharging step. Indeed, the insulant rises in temperature during the charge, and is

still hot during the discharge. When the TES material cools down, the insulation is able to give the energy back to the system.

At the end of the charging, 89% of the energy provided by the inlet hot air was stored by the TES material. This illustrates a reliable charging process at industrial scale, with a technico-economical compromise between the load ratio and the energy lost as hot air.

5.1.4. Storage yield

Storage yield is the crucial parameter for the evaluation of a waste heat recovery system. As defined in Eqs. (8) and (9), both global and local storage yields are used. Plotting these parameters against discharge threshold temperature allows showing how the heat quality is affected by the storage process. It underlines the impact of the horizontal geometry and shape of the storage tank on the performances of the storage system (Figure 9).

The local storage yield (Figure 9 a) represents the packed bed ability between section A and section C to recover heat. The discharge threshold temperature depends on downstream process. As expected, decreasing the threshold temperature allows increasing local storage yield. This latter reached 91% for a discharge threshold temperature of 200°C, where the discharge was stopped during discharging step of this experiment. This means 91% of heat stored between the section A and section C could be released above 200°C. Increasing the threshold temperature to 350, 450 and 525°C would lead to the local storage yield of respectively 81, 68 and 40%. Therefore, the energy indicators strongly depend on the capacity of the process to admit variable temperatures. A choice has to be made between quantity and quality of the heat recovered, chosen by the cutoff temperature.

The local storage yield could be relatively well modelled. Some difference between numerical and experimental approach at high threshold temperature could be explained by errors of temperature measurement.

The global storage yield (Figure 9 b) completes the information given by the local storage yield. Indeed, it takes all the elements of the TES system into account, including the piping and the diffusers where thermal inertia or thermal losses could happen. However, the global storage yield was specific to this particular setup, and reached 83%, when the discharged was stopped. At this moment, the global outlet temperature was 50°C higher than the local outlet temperature measured at the section A, which is possibly due to the 100 mm of packed layer located downstream section A, coupled with the thermal inertia of the piping. This inertia could likely have an impact on industrial implementations equipped with long piping. A particular attention should be paid to the insulation of the piping in this case.

5.1.5. Wall thermal loss

When the discharged stops at 200°C, 1.78 MWh_{Th} of heat is discharged, and 0.07 MWh_{Th} remains in the packed bed since the thermocline is not completely extracted from the TES. It is possible to approximate wall thermal losses during the discharge, using eq. 14. This wall thermal losses is part of $Q_{lateral}$.

$$Q_{loss_{wall-d}} = Q_{bau}(t_{end-ch}) + Q_{lateral}(t_{end-ch}) - (Q_{exc-d}(t_{end-d}) + Q_{bau}(t_{end-d})) \quad (19)$$

where: $Q_{bau}(t_{end\text{-}ch})$ is energy stored by the TES material; $Q_{lateral}(t_{end\text{-}ch})$ is energy stored by the insulant; $Q_{exc\text{-}d}(t_{end\text{-}d})$ is the discharged energy, and $Q_{bau}(t_{end\text{-}d})$ is the residual energy remaining in the storage tank.

So, $Q_{loss\_wall\text{-}d}$ represents the wall thermal losses during the discharging step, that is estimated to 1.0% of $Q_{exc\text{-}d}$, the energy discharged. The storage was therefore properly insulated.

However, significant losses occurred in the piping of the setup, with a global storage yield of 83.4%. So, the insulation of the air duct plays important role to limit the heat loss from waste heat source to TES tank (for the charging step) and from the TES tank to the deliverance point (for the discharging step).

5.2. Cycling test

The first results show that the performances of the containerized storage unit do not show specific behavior linked to the horizontal configuration during single standard charge and discharge (with a constant flowrate and temperature source). Nevertheless, during cycling operation, phenomenon such as natural convection is more likely to appear, resulting in de-stratification of the thermocline. That is why the impact of cycling operation on the horizontal storage has also been evaluated.

5.2.1. Temperature evolution

The Eco-Stock® is generally not completely discharged since the downstream process defines the threshold discharging temperature. The energy remaining after a discharging step reduces energy needed to

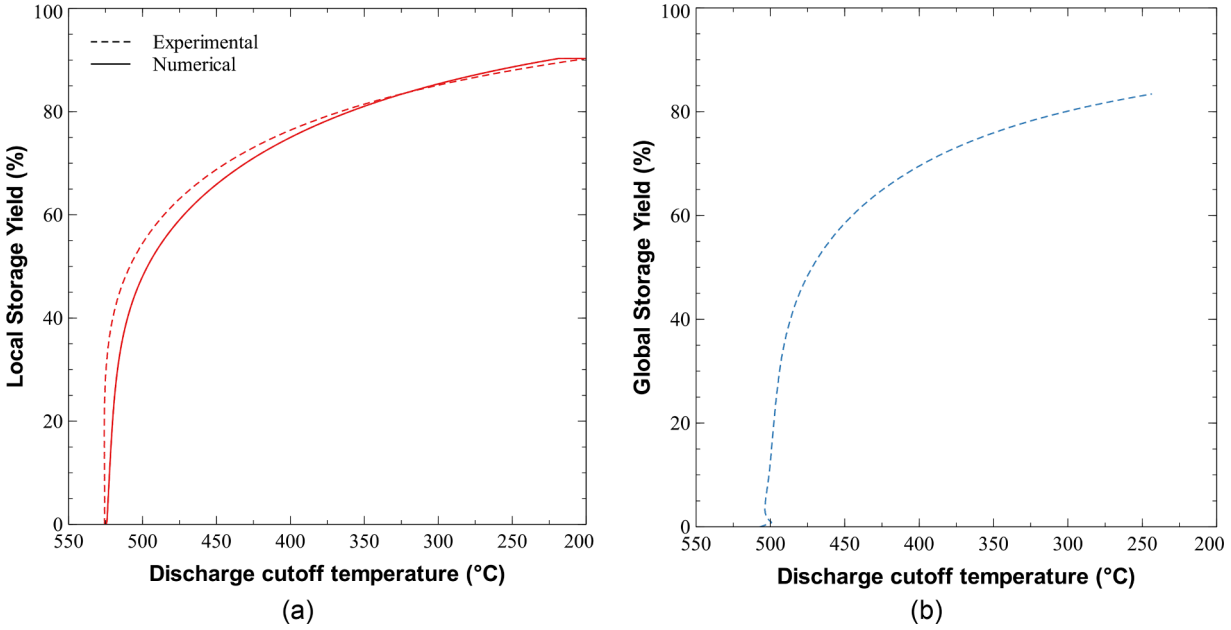

Figure 9. Local storage yield (a) and global storage yield (b) as a function of the discharge threshold temperature during the discharging step.

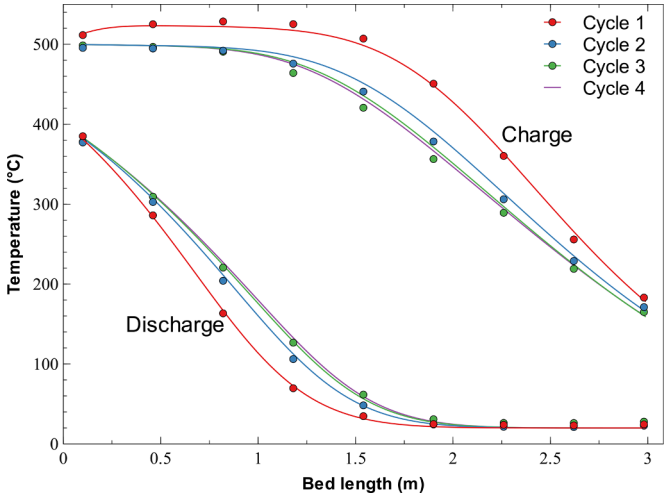

Figure 10. Temperature profiles at the start and the end of each cycle. Continuous lines: numerical values; points: experimental results.

charge the TES system of the next cycle, but it also increases the de-stratification of the thermocline. Reaching a permanent cycle depends on the threshold temperature of charge and discharge [30]. Repeated charging/discharging cycles are performed on the Eco-Stock®. The system is charged then discharged 3 times in a row to observe the stabilization of its performances along the cycles. The threshold temperature arbitrarily set at 170°C and 380°C respectively.

A technical issue happened during the first cycle at the 5th hour. The charging temperature was reduced from 525°C to 500°C during the rest of the 1st charge. The 500°C charging temperature was kept until the end of the test (2nd and 3rd cycle). The impact of the 20°C decrease is taken into account in the numerical model. The charging and discharging flowrate were 0.58 kg.s^{-1} and 0.65 kg.s^{-1} respectively, for all cycles.

Figure 10 shows the temperature profiles of the TES tank at the end of each charge and discharge obtained from both numerical simulation and experimental measurement, and the characteristics of each cycle are presented in Table 2.

The de-stratification is visible between the cycles, with a decrease of the temperature slope. The increase of the thermocline length implies to reach threshold temperatures more rapidly, and therefore reduces the charging time and the storage capacity. Thus, for the same threshold temperatures, the load ratio decreased from 75% to 62% during three cycles (Table 2). The duration of the charging step was also reduced from 11.25 h for the first cycle to 8.15 h for the third cycle. A smaller reduction of discharging time is also observed. The temperature of the TES tank was well modeled, with a maximum of 10 and 5°C of difference for the charge and discharge, respectively. The industrial thermal storage confirms that with loose threshold temperature ($\theta_{threshold\text{-}ch}$ = 0.75 and $\theta_{threshold\text{-}d}$ = 0.31), the temperature profiles could be stable after only a few cycles. Fasquelle *et al.* showed that 3 cycles can be enough to reach a permanent state with similar operating conditions ($\theta_{threshold\text{-}ch}$ = 0.7 and $\theta_{threshold\text{-}d}$ = 0.3) but with oil as HTF [30]. Three cycles were not enough in this study for the temperature profile to be perfectly overlapped, which could be explained by the higher charging temperature during the first cycle. In fact, numerical results show that this system may be stabilized after the 4th cycle.

5.2.2. Storage Yield

As for the single charge-discharge, the performances of the storage during cycling operation could be altered by the geometry of the tank. Since the local storage yield is the main performance indicator, it is plotted for the 3 cycles.

Figure 11 shows the local storage yield as a function of the outlet air temperature during the 3 cycles, obtained by both experimental measurement and numerical simulation. For all 3 cycles, the numerical code is able to model properly the local storage yield. For the 1st discharge, the outlet air temperature starts at 512°C because the charging temperature was reduced at the end of the 1st cycle due to a technical issue. The measured temperature then reaches 525°C. For the 2nd and 3rd discharges, the outlet air temperature reaches up 500°C which is also the charging temperature of these cycles. Figure 11 shows that the Eco-Stock® seems to be stabilized between the 2nd and the 3rd cycle (respectively C2 and C3 curves), with a maximum of 2% difference. It shows that the behavior of the tank tends to stabilize in a few cycles for those operating conditions. The local storage yield is increased from 77% for the 1st cycle to 90% for the 3rd cycle. This is due to the energy remaining inside the TES tank at the end of each discharge, which reduces the energy required for the following charging step, Q_{air-ch}, from 1.99 MWh_{Th} for the 1st cycle to 1.45 MWh_{Th} for the 3rd cycle. During cycling operation, up to 90% of the available energy can be recovered, proving the ability of the thermal storage at industrial scale to store and deliver heat.

Table 2
Cycle characteristics.

Cycle	1	2	3
Charging time (h)	11.45	8.98	8.25
Discharging time (h)	4.62	4.02	3.75
Load ratio (%)	75	67	62
Idle phase between charge and discharge (min)	25	16	9
Idle phase between discharge and next charge (min)	8	3	-

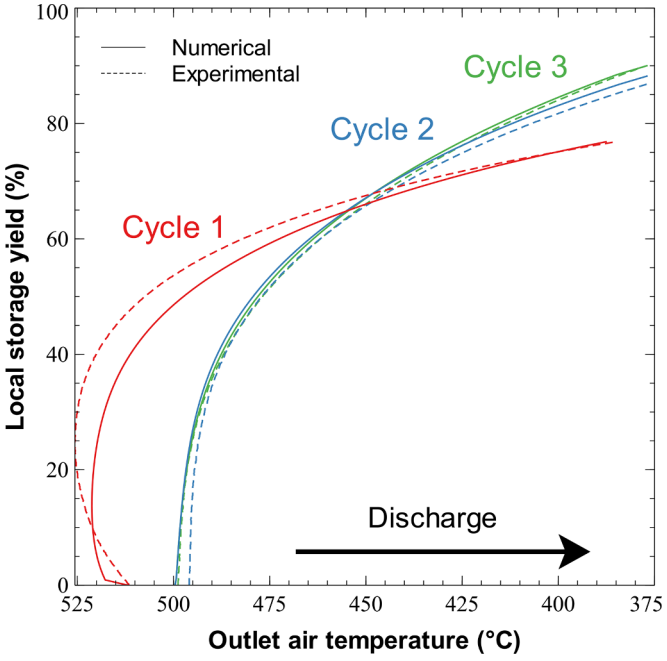

Figure 11. Local storage yield obtained by both experimental measurement and numerical simulation.

6. Conclusions

An industrial-scale air-ceramic horizontal packed-bed TES, of dimensions 1.7 × 1.7 × 3.08 m^3 was designed and built by Eco-Tech Ceram to recover waste heat. This singular unit presents a horizontal and containerized geometry, to enable easy transportation and implementation. The Eco-Stock® was able to store 1.9 MWh_{Th} of heat at 525°C (charged at 300 kW_{Th}, discharged 350 kW_{Th}), which validates the performances of a commercial TES operating in real conditions. The

concept of horizontal thermocline TES at industrial scale is validated with performance indicators specific to waste heat. This validation encourages the deployment of the technology for waste heat recovery applications.

The horizontal thermocline TES was tested with three continuous charging/discharging cycles with inlet charging temperature of 525-500°C. The results showed that this Eco-Stock® was able to recover up to 90% of the heat source with a discharge threshold temperature of 200°C, indicating high performance of the designed system. No channeling effect and only moderate radial effects due to the horizontal configuration could be detected. This homogenization comes from the packed bed itself and a length of a few particle diameters are probably necessary to homogenize the mass flow over the section. The plug and play TES studied here presents a non-negligible part of its energy stored in its insulant, which is recovered. To take into account such phenomenon, a one-dimension 3-temperature model is proposed. Also, the numerical model fitted well experimental data and the temperature profile of the storage tank could be predicted, with a RMSD below 20°C.

Future work will focus on the development of Eco-Stock® operating at higher temperature (above 1000°C). This would allow to recover high temperature waste heat as well as to couple TES with concentrated solar towers to increase the dispatchability of CSP plants.

CRediT authorship contribution statement

Aubin Touzo: Methodology, Investigation, Software, Writing - original draft. **Régis Olives:** Conceptualization, Methodology, Writing - review & editing. **Guilhem Dejean:** Conceptualization, Resources, Writing - review & editing. **Doan Pham Minh:** Methodology, Writing - review & editing. **Mouna El Hafi:** Supervision, Project administration, Writing - review & editing. **Jean-François Hoffmann:** . **Xavier Py:** Supervision, Project administration, Funding acquisition.

Declaration of Competing Interest

The authors declare that they have no known competing financial interests or personal relationships that could have appeared to influence the work reported in this paper.

Acknowledgments

This project has received funding from the programme “investissement d'avenir” (investments for the future) of the “Agence Nationale de la Recherche” (National Agency for Research) of the French state under award number” ANR-10-LBX-22-01-SOLSTICE, and from BPI France from the World Innovation Competition Phase 2 for the Eco-Stock® project. The authors would like to thank Yoann Le Blevennec for his help in the study.

References

[1] ADEME, La chaleur fatale industrielle. Connaître pour agir, (2015). http://www.ademe.fr/sites/default/files/assets/documents/ademe-chaleur-fatale-industrielle-8445-2015-03.pdf.
[2] U.S. Department of Energy, Waste heat Recovery: Technology and Opportunities in U. S. Industry, U.S. Dep. Energy, Ind. Technol. Progr. (2008).
[3] L. Miró, J. Gasia, L.F. Cabeza, Thermal energy storage (TES) for industrial waste heat (IWH) recovery: A review, Appl. Energy 179 (2016) 284–301 https://doi.org/10.1016/j.apenergy.2016.06.147.
[4] U. Pelay, L. Luo, Y. Fan, D. Stitou, M. Rood, Thermal energy storage systems for concentrated solar power plants, Renew. Sustain. Energy Rev. 79 (2017) 82–100 https://doi.org/10.1016/j.rser.2017.03.139.
[5] G. Angelini, A. Lucchini, G. Manzolini, Comparison of thermocline molten salt storage performances to commercial two-tank configuration, Energy Procedia 49 (2013) 694–704 https://doi.org/10.1016/j.egypro.2014.03.075.
[6] S.S. Mostafavi Tehrani, R.A. Taylor, K. Nithyanandam, A. Shafiei Ghazani, Annual comparative performance and cost analysis of high temperature, sensible thermal energy storage systems integrated with a concentrated solar power plant, Sol. Energy 153 (2017) 153–172 https://doi.org/10.1016/j.solener.2017.05.044.
[7] X. Py, N. Calvet, R. Olives, A. Meffre, P. Echegut, C. Bessada, E. Veron, S. Ory, Recycled Material for Sensible Heat Based Thermal Energy Storage to be Used in Concentrated Solar Thermal Power Plants, J. Sol. Energy Eng. 133 (2011) 031008https://doi.org/10.1115/1.4004267.
[8] M.E. Navarro, M. Martínez, A. Gil, A.I. Fernández, L.F. Cabeza, R. Olives, X. Py, Selection and characterization of recycled materials for sensible thermal energy storage, Sol. Energy Mater. Sol. Cells. 107 (2012) 131–135 https://doi.org/10.1016/j.solmat.2012.07.032.
[9] S. Zunft, M. Hänel, M. Krüger, V. Dreißigacker, F. Göhring, E. Wahl, Jülich Solar Power Tower—Experimental Evaluation of the Storage Subsystem and Performance Calculation, J. Sol. Energy Eng. 133 (2011) 031019https://doi.org/10.1115/1.4004358.
[10] G. Zanganeh, A. Pedretti, S. Zavattoni, M. Barbato, A. Steinfeld, Packed-bed thermal storage for concentrated solar power - Pilot-scale demonstration and industrial-scale design, Sol. Energy 86 (2012) 3084–3098 https://doi.org/10.1016/j.solener.2012.07.019.
[11] L. Geissbühler, V. Becattini, G. Zanganeh, S. Zavattoni, M. Barbato, A. Haselbacher, A. Steinfeld, Pilot-scale demonstration of advanced adiabatic compressed air energy storage, Part 1: Plant description and tests with sensible thermal-energy storage, J. Energy Storage 17 (2018) 129–139 https://doi.org/10.1016/j.est.2018.02.004.
[12] B.S. Thibaut Esence, Tristan Desrues, Jean-François Fourmigué, Grégory Cwicklinski, Arnaud Bruch, Experimental study and numerical modelling of high temperature gas/solid packed-bed heat storage systems, Energy (2019) 1–22.
[13] T. Esence, T. Desrues, J.F. Fourmigué, G. Cwicklinski, A. Bruch, B. Stutz, Experimental study and numerical modelling of high temperature gas/solid packed-bed heat storage systems, Energy 180 (2019) 61–78 https://doi.org/10.1016/j.energy.2019.05.012.
[14] T. Esence, A. Bruch, S. Molina, B. Stutz, J.F. Fourmigué, A review on experience feedback and numerical modeling of packed-bed thermal energy storage systems, Sol. Energy 153 (2017) 628–654 https://doi.org/10.1016/j.solener.2017.03.032.
[15] J.F. Hoffmann, T. Fasquelle, V. Goetz, X. Py, A thermocline thermal energy storage system with filler materials for concentrated solar power plants: Experimental data and numerical model sensitivity to different experimental tank scales, Appl. Therm. Eng. 100 (2016) 753–761 https://doi.org/10.1016/j.applthermaleng.2016.01.110.
[16] I. Ortega-Fernández, Y. Wang, M. Durán, E. Garitaonandia, L. Unamunzaga, D. Bielsa, E. Palomo, Experimental validation of steel slag as thermal energy storage material in a 400 kWht prototype, AIP Conf. Proc. 2126 (2019) 4–5 https://doi.org/10.1063/1.5117741.
[17] T. Fasquelle, Q. Falcoz, P. Neveu, J.F. Hoffmann, A temperature threshold evaluation for thermocline energy storage in concentrated solar power plants, Appl. Energy 212 (2018) 1153–1164 https://doi.org/10.1016/j.apenergy.2017.12.105.
[18] N. Lopez Ferber, Q. Falcoz, D. Pham Minh, J.F. Hoffmann, A. Meffre, A. Nzihou, V. Goetz, Flexibility and robustness of a high-temperature air/ceramic thermocline heat storage pilot, J. Energy Storage 21 (2019) 393–404 https://doi.org/10.1016/j.est.2018.11.034.
[19] M.M.S. Al-Azawii, C. Theade, M. Danczyk, E. Johnson, R. Anderson, Experimental study on the cyclic behavior of thermal energy storage in an air-alumina packed bed, J. Energy Storage 18 (2018) 239–249 https://doi.org/10.1016/j.est.2018.05.008.
[20] S. Soprani, F. Marongiu, L. Christensen, O. Alm, K.D. Petersen, T. Ulrich, K. Engelbrecht, Design and testing of a horizontal rock bed for high temperature thermal energy storage, Appl. Energy 251 (2019) 113345https://doi.org/10.1016/j.apenergy.2019.113345.
[21] C. Odenthal, W.D. Steinmann, S. Zunft, Analysis of a horizontal flow closed loop thermal energy storage system in pilot scale for high temperature applications – Part II: Numerical investigation, Appl. Energy 263 (2020) 114576https://doi.org/10.1016/j.apenergy.2020.114573.
[22] C. Odenthal, W.D. Steinmann, S. Zunft, Analysis of a horizontal flow closed loop thermal energy storage system in pilot scale for high temperature applications – Part I: Experimental investigation of the plant, Appl. Energy 263 (2020) 114573https://doi.org/10.1016/j.apenergy.2020.114573.
[23] H. Agalit, N. Zari, M. Maalmi, M. Maaroufi, Numerical investigations of high temperature packed bed TES systems used in hybrid solar tower power plants, Sol. Energy 122 (2015) 603–616 https://doi.org/10.1016/j.solener.2015.09.032.
[24] K.A.R. Ismail, R. Stuginsky, Parametric study on possible fixed bed models for pcm and sensible heat storage, Appl. Therm. Eng. 19 (1999) 757–788 https://doi.org/10.1016/S1359-4311(98)00081-7.
[25] J.F. Hoffmann, T. Fasquelle, V. Goetz, X. Py, Experimental and numerical investigation of a thermocline thermal energy storage tank, Appl. Therm. Eng. 114 (2017) 896–904 https://doi.org/10.1016/j.applthermaleng.2016.12.053.
[26] S.S. Sih, J.W. Barlow, The prediction of the emissivity and thermal conductivity of powder beds, Part. Sci. Technol. 22 (2004) 427–440 https://doi.org/10.1080/02726350490501682.
[27] M. Díaz-Heras, J.F. Belmonte, J.A. Almendros-Ibáñez, Effective thermal conductivities in packed beds: Review of correlations and its influence on system performance, Appl. Therm. Eng. 171 (2020) 115048https://doi.org/10.1016/j.applthermaleng.2020.115048.
[28] N. Lopez Ferber, PhD Thesis, (2018).
[29] A.S.A. Ammar, A.A. Ghoneim, Optimization of a sensible heat storage unit packed with spheres of a local material, Renew. Energy 1 (1991) 91–95 https://doi.org/10.1016/0960-1481(91)90107-Z.
[30] T. Fasquelle, PhD Thesis, (2017).